AD-A049 537 AERONAUTICAL RESEARCH ASSOCIATES OF PRINCETON INC N J F/G 21/2
A REACTING TURBULENT BOUNDARY LAYER APPROACH TO SOLID PROPELLAN--ETC(U)
NOV 77 R A BEDDINI F44620-76-C-0016
UNCLASSIFIED ARAP-319 AFOSR-TR-77-1310 NL

1 OF 1
ADA049537

END
DATE FILMED
3-78
DDC

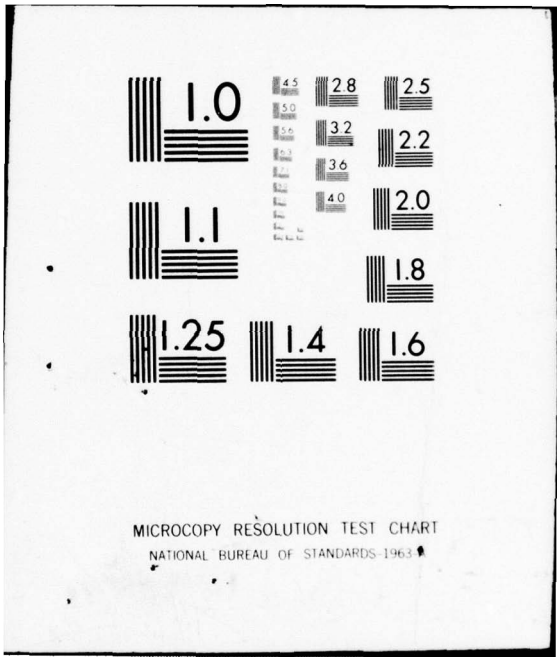
1.0
1.1
1.25
1.4
1.6
1.8
2.0
2.2
2.5
2.8
3.2
3.6
4.0
4.5
5.0
5.6
6.3
MICROCOPY RESOLUTION TEST CHART
NATIONAL BUREAU OF STANDARDS-1963-A

AFOSR-TR- 77-1310

(2) B.S.

A REACTING TURBULENT BOUNDARY LAYER APPROACH TO SOLID PROPELLANT EROSIVE BURNING

ROBERT A. BEDDINI

008400

wse

AERONAUTICAL RESEARCH ASSOCIATES OF PRINCETON, INC.
50 WASHINGTON ROAD, P.O. BOX 2229
PRINCETON, NEW JERSEY 08540

NOVEMBER 1977

FINAL SCIENTIFIC REPORT
FOR THE PERIOD 1 OCTOBER 76 - 30 SEPTEMBER 1977

PREPARED FOR

AIR FORCE OFFICE OF SCIENTIFIC RESEARCH (AFSC)
BUILDING 410, BOLLING AIR FORCE BASE
WASHINGTON, DC 20332

APPROVED FOR PUBLIC RELEASE; DISTRIBUTION UNLIMITED

SECURITY CLASSIFICATION OF THIS PAGE (When Data Entered)

REPORT DOCUMENTATION PAGE

READ INSTRUCTIONS BEFORE COMPLETING FORM

1. REPORT NUMBER: AFOSR-TR-77-1310	2. GOVT ACCESSION NO.
3. RECIPIENT'S CATALOG NUMBER	
4. TITLE (and Subtitle): A REACTING TURBULENT BOUNDARY LAYER APPROACH TO SOLID PROPELLANT EROSIVE BURNING	5. TYPE OF REPORT & PERIOD COVERED: FINAL scientific rept. 1 Oct 76 - 30 Sep 77
6. PERFORMING ORG. REPORT NUMBER: ARAP [redacted] 319	
7. AUTHOR(s): ROBERT A. BEDDINI	8. CONTRACT OR GRANT NUMBER(s): F44620-76-C-0016
9. PERFORMING ORGANIZATION NAME AND ADDRESS: ARAP OF PRINCETON, INC 50 WASHINGTON RD/PO BOX 2229 PRINCETON, NJ 08540	10. PROGRAM ELEMENT, PROJECT, TASK AREA & WORK UNIT NUMBERS: 2308 A1 / A1 / 61102F
11. CONTROLLING OFFICE NAME AND ADDRESS: AIR FORCE OFFICE OF SCIENTIFIC RESEARCH/NA BLDG 410 BOLLING AIR FORCE BASE, D C 20332	12. REPORT DATE: Nov 77 13. NUMBER OF PAGES: 43 / 46 P.
14. MONITORING AGENCY NAME & ADDRESS (if different from Controlling Office)	15. SECURITY CLASS. (of this report): UNCLASSIFIED 15a. DECLASSIFICATION/DOWNGRADING SCHEDULE

16. DISTRIBUTION STATEMENT (of this Report)

Approved for public release; distribution unlimited.

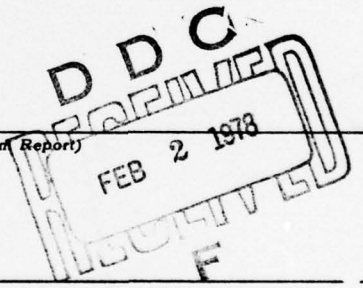

17. DISTRIBUTION STATEMENT (of the abstract entered in Block 20, if different from Report)

18. SUPPLEMENTARY NOTES

19. KEY WORDS (Continue on reverse side if necessary and identify by block number)

EROSIVE BURNING
TURBULENT BOUNDARY LAYERS-REACTING
SOLID PROPELLANTS
SECOND-ORDER CLOSURE
AEROTHERMOCHEMISTRY

20. ABSTRACT (Continue on reverse side if necessary and identify by block number)

A theoretical analysis of the erosive burning of solid propellants is presented using a reacting turbulent boundary layer approach. The turbulent field is modeled using the second-order closure technique and a single-step gas-phase reaction is assumed for the combustion of a homogeneous propellant. The calculated results agree with the generally observed erosive burning trends of threshold velocity, nonlinear recession-ratio velocity dependence, pressure dependence, and normal burning rate sensitivity. For constant external velocity boundary layers, the results show a decrease in burning rate along the propellant surface, which also has been observed experimentally. Examination of

DD FORM 1 JAN 73 1473 EDITION OF 1 NOV 65 IS OBSOLETE

UNCLASSIFIED

SECURITY CLASSIFICATION OF THIS PAGE (When Data Entered)

008 400

calculated profiles of temperature and turbulent correlations in the boundary layer reveals that erosive burning is predominantly caused by flame zone broadening due to the diffusive effects of turbulence.

FOREWORD

This final report is furnished for Air Force Office of Scientific Research on Contract No. F44620-76-C-0016. Aeronautical Research Associates of Princeton, Inc., will continue its erosive burning research under sub-contract to Atlantic Research Corporation, funded by Air Force Office of Scientific Research on prime Contract No. F49620-78-C-0016.

A REACTING TURBULENT BOUNDARY LAYER APPROACH TO SOLID PROPELLANT EROSIVE BURNING

Robert A. Beddini*

Aeronautical Research Associates of Princeton, Inc.
Princeton, New Jersey 08540

ABSTRACT

A theoretical analysis of the erosive burning of solid propellants is presented using a reacting turbulent boundary layer approach. The turbulent field is modeled using the second-order closure technique and a single-step gas-phase reaction is assumed for the combustion of a homogeneous propellant. The calculated results agree with the generally observed erosive burning trends of threshold velocity, nonlinear recession-ratio velocity dependence, pressure dependence, and normal burning rate sensitivity. For constant external velocity boundary layers, the results show a decrease in burning rate along the propellant surface, which also has been observed experimentally. Examination of calculated profiles of temperature and turbulent correlations in the boundary layer reveals that erosive burning is predominantly caused by flame zone broadening due to the diffusive effects of turbulence.

---

*Associate Consultant, Member AIAA

Originally presented as AIAA paper No. 77-931, AIAA/SAE 13th Propulsion Conference, July 1977.

Research supported by the Air Force Office of Scientific Research under Contract No. F44620-76-C-0016; Major Thomas C. Meier, Program Manager.

NOMENCLATURE

A	Arrhenius pre-exponential coefficient
c_p	specific heat at constant pressure
c_π	specific heat of propellant
D	overall diffusion coefficient
$g_{\ell m}$	metric tensor, $\partial x_\ell / \partial x_m$
h	specific sensible enthalpy
h_α^o	heat of formation at $0^\circ K$
H	total enthalpy, $H = h + u^i u_i/2$
k	thermal conductivity
L_s^o	heat of decomposition at $0^\circ K$
$\dot{m}_s$	surface mass flux
n	normal burning rate pressure exponent
n_j	surface normal vector
p	hydrostatic pressure
p_*	reference pressure, 6.9×10^7 dyne/cm^2 (1000 psi)
$\dot{q}_j$	heat transfer vector
$\dot{r}$	recession (burning) rate, $\dot{m}_s/\rho_\pi$
$\dot{r}_n$	normal (nonerosive) recession rate
$\dot{r}_*$	$\dot{r}_n(p_*)$
R	gas constant per unit mole
s	width of two-dimensional channel
S_α	symbol of chemical species α
t	time
T	temperature
T_A	activation temperature (energy/R)

NOMENCLATURE (cont.)

T_i	interior propellant temperature
u_j	velocity vector {u,v,w}
U_e	velocity external to boundary layer
U_e^o	$U_e(x = 0)$
$\dot{w}_\alpha$	rate of production of species α per unit mass
W_α	molecular weight of species α
x_j	coordinate vector {x,y,z}
Y_α	mass fraction
β	temperature exponent of reaction pre-exponential coefficient
Δh_g	heat of reaction per unit mass
Λ	turbulent macrolength scale
μ	viscosity
ξ	length of initial adiabatic surface
ρ	density
ϕ	$\sum_\alpha \nu_\alpha'' W_\alpha$
Φ	concentration (pressure) exponent in reaction rate

Superscripts

$\overline{\quad}$	denotes time average of variable
'	denotes turbulent fluctuating value of variable

Subscripts

F	fuel
g	gas phase
e	value external to boundary layer
O	oxidizer
s	propellant surface value

NOMENCLATURE (cont.)

α	index for chemical species
π	denotes propellant solid phase
o	stagnation value
,	denotes differentiation

INTRODUCTION

The term "erosive burning" refers to the increase in solid propellant burning rate in the presence of a convective flow parallel to the propellant surface. Most current motor designs utilize a central port within the propellant grain through which the combustion gases flow. As the flow velocity increases toward the aft end of the port, a position is reached where the propellant burning rate due to erosion may exceed the normal (strand) burning rate by several percent.[1] This increase must be accurately accounted for in the prediction of overall motor thrust performance. In addition, recent design trends to high port velocity ($M \simeq 1$) and nozzleless rocket motors further accentuate this problem.[2]

Literature reviews of erosive burning observations and theoretical treatments have been reported in Williams, et al.[1] King[2] and Kuo and Razdan.[3] Various mechanisms have been hypothesized to account for erosive burning behavior. For example, the mechanism first proposed by Corner[4] is that the turbulent boundary layer on the surface of the propellant increases the effective thermal diffusivity in the flame zone, thus increasing heat transfer to the propellant. This hypothesis is used in several erosive burning theories, including those of Vandenkerckhove[5] (for homogeneous propellants) and Lengelé[6] (for composite propellants). A substantially different cause of erosive burning was proposed by Lenoir and Robillard,[7] and has since been diversely applied.[1,2] Lenoir and Robillard maintain that erosive burning is caused by the increased surface heat transfer from the hot "core" gas external to the boundary layer, and add this effect to the normal burning rate. This proposed cause has been criticized by

King, who notes that the strong dependence on core gas temperature exhibited by the theory is contradicted by experimental observations. King develops an alternative theory for composite propellant erosive burning which is based on the mechanism of convective bending of the diffusion-controlled flame zone. As the total combustion length scale is assumed constant, the resulting flame zone lies closer to the propellant surface and provides increased heat transfer.

The preceding theories are here termed of integral type and offer the advantage of providing solutions for surface recession (burning) rate in relatively simple algebraic forms. However, they have two major disadvantages. If the supposed physical cause of erosive burning is erroneous, the theoretical method constructed upon the cause will obviously be of questionable predictive utility. The second disadvantage of integral theories at their present stage of development is that they invoke rather tenuous assumptions concerning boundary layer profiles in the flame zone. For example, the theories of Lengelé and King use incompressible turbulent velocity profiles in a region where the gas density is typically changing by a factor of three. If the effects of compressibility on heat transfer and streamwise-velocity profile for high speed boundary layers[8] are indicative of density effects on propellant boundary layers, then the potential for large error exists in these theories. The accuracy of the velocity profile description (whether affected by density or other source) directly affects the results of Lengelé, since the erosive contribution to burning rate is assumed proportional to velocity gradient. The flame bending model of King is also quite sensitive to velocity

profile, although with nonlinear dependence. Additionally, King's model is somewhat inconsistent in accounting for turbulence effects on the mean velocity field, but not on the mean temperature field.

An approach to erosive burning is needed which avoids predication on a specific cause and is not subject to the severe approximations used in contemporary integral theories. Therefore, an analysis of the basic differential equations appropriate for a reacting boundary layer flow is pursued. This type of analysis has been termed an aerothermochemical approach in the prior laminar-flow studies of Tsuji[9] and Schuyler and Torda.[10] The objectives of the present study are to investigate the role of turbulence in erosive burning, and to qualitatively validate the basic approach through comparison with several observed erosive burning trends. The approach accounts for the effects of turbulence on boundary layer heat, mass, and momentum transfer through use of the second-order turbulence closure technique.[11] A single-step gas-phase reaction is assumed for the combustion of a homogeneous propellant. This type of reaction mechanism is believed adequate for trend analysis, as reviews of erosive burning experimental observations[1,3] indicate that several trends are common to both homogeneous and composite propellants.

ANALYSIS

Figure 1 shows the geometry under consideration, which is quite similar to the proposed experimental apparatus of Razdan and Kuo.[12] A boundary layer develops along an adiabatic surface of length ξ, and undergoes transition to turbulent flow before encountering the propellant. Due to approximations which will be imposed in this section, the composition and total enthalpy of the initial "driver" flow are taken to be identical to those of the test propellant combustion products. The two-dimensional, symmetric channel through which the combustion gases flow is assumed to be maintained at constant width, s.

The fundamental differential equations are adapted from Williams.[13] A single species diffusion coefficient is assumed, and the effects of thermodiffusion and bulk viscosity are neglected. General tensor notation[14] is used to aid in the manipulations required for turbulence analysis, and to extend the validity of the analysis to axisymmetric flow. Covariant differentiation, and differentiation with respect to scalar variables, is denoted by a comma. The species index α consistently ranges from 1 through N. The equations for conservation of mass, momentum, species mass fraction, total enthalpy, and the equation of state are:

$$\rho_{,t} + (\rho u^{\ell})_{,\ell} = 0 \tag{1}$$

$$\rho(u_{j,t} + u^{\ell}u_{j,\ell}) = -p_{,\ell} + g^{\ell m}\left[\mu(u_{j,m} + u_{m,j})\right]_{,\ell} \tag{2}$$

$$(\rho Y_{\alpha})_{,t} + (\rho u^{\ell} Y_{\alpha})_{,\ell} = g^{\ell m}(\rho D Y_{\alpha,m})_{,\ell} + \dot{w}_{\alpha} \tag{3}$$

$$(\rho H)_{,t} + (\rho u^{\ell} H)_{,\ell} = g^{\ell m}\Big[kT_{,m} + \rho D \sum_{\alpha} h_{\alpha} Y_{\alpha,m} + 1/2\,(u^{i}u_{i})_{,m}\Big]_{,\ell} - \sum_{\alpha} h_{\alpha}^{o}\dot{w}_{\alpha} + p_{,t} + (\mu u^{m} u^{\ell}_{,m})_{,\ell} \quad (4)$$

$$p = \rho RT \sum_{\alpha} Y_{\alpha}/W_{\alpha} \quad (5)$$

For the present analysis, the following assumptions are initially invoked:

a) Specific heats of the species are equal and independent of temperature

b) $k/c_p = \rho D = \mu(T)$

c) Combustion of the stoichiometric mixture proceeds through the single-step reaction

$$\sum_{\alpha} \nu'_{\alpha} S_{\alpha} \rightarrow \sum_{\alpha} \nu''_{\alpha} S_{\alpha}$$

where S_{α} are the symbols of the N chemical species, and ν'_{α} and ν''_{α} are the stoichiometric coefficients of reactants and products. Specifically considered is the reaction Fuel + Oxidizer → Products, for which the chemical production term is of the form

$$\dot{w}_{\alpha} = (\nu''_{\alpha} - \nu'_{\alpha}) W_{\alpha} \omega$$

with ω assumed as

$$\omega = A_g T^{\beta_g} \exp(-T_{Ag}/T)(\rho Y_F/W_F)^{\Phi_F}(\rho Y_O/W_O)^{\Phi_O}$$

Assumptions (a) - (c) are often invoked in combustion theory and include the approximations of Shvab-Zeldovich.[13] With regard to assumption (c), the concentration exponents Φ_F and Φ_0 have not been restricted to be stoichiometric, as is usually done.[1,9,13] In this way, the concentration exponents may be selected to better approximate the reaction pressure-dependence within the constraint of the single-step reaction. Nonstoichiometric values of Φ_F and Φ_0 have been experimentally observed to provide a good approximation to an overall reaction rate for simple systems over a specified pressure range.[15]

The immediate objective in using the assumptions is to linearly relate the mass fractions to the total enthalpy. This has been done in the case of normal propellant burning by Johnson and Nachbar,[16] and in the laminar aerothermochemical analysis of Tsuji. To achieve this condition of similarity in turbulent flow, consideration must be given to the boundary conditions at the solid surface and boundary layer edge in a general coordinate system. This is necessary to provide consistency with the differential equations prior to Reynolds (time) averaging and the imposition of boundary layer assumptions.

Following Johnson and Nachbar, reference mass fractions $Y_{\alpha *}$ are defined at the initial state of the reaction such that

$$Y_{\alpha *} = \nu'_\alpha W_\alpha / \phi \tag{6}$$

where

$$\phi = \sum_\alpha \nu'_\alpha W_\alpha = \sum_\alpha \nu''_\alpha W_\alpha$$

The mass fractions at the end state of the reaction (equivalently, external to the boundary layer) are

$$Y_{\alpha e} = \nu''_{\alpha} W_{\alpha}/\phi \tag{7}$$

The propellant-gas interface boundary conditions for Y_α and H, as adapted from Williams are

$$\dot{m}_s(Y_{\alpha s} - Y_{\alpha *}) = \rho D n^j Y_{\alpha,j}\Big|_s \tag{8}$$

$$\dot{m}_s L_s - n^j \dot{q}_{\pi j}\Big|_s = \frac{k}{c_p} n^j H_{,j}\Big|_s \tag{9}$$

In the above equations $\dot{m}_s = \rho u_j n^j\Big|_s$ is the surface mass flux, n^j is the unit vector normal to the propellant surface, L_s is the heat of decomposition between the solid and gas states (defined negative for exothermic heat of decomposition) and $\dot{q}_{\pi j}$ is the heat flux vector out of the propellant. Nonadiabatic processes (e.g., radiation) have been excluded from Eq. (9). If it is assumed at this stage that the heat flux in the propellant is one-dimensional, steady, and occurs in a thin layer, then

$$-n^j \dot{q}_{\pi j}\Big|_s = \dot{m}_s c_\pi (T_s - T_i)$$

The heat of decomposition is taken to be of the form appropriate for a "perfect" substance[17]

$$L_s = L_s^o + (c_p - c_\pi)T_s \tag{10}$$

The asymptotic boundary conditions for species and total enthalpy at the edge of the boundary layer are given by Eq. (7) for Y_α, and by an overall energy balance for H. Defining the heat of reaction (energy/unit mass of product) as

$$\Delta h_g = \phi^{-1} \sum_\alpha (\nu'_\alpha - \nu''_\alpha) W_\alpha h^o_\alpha = \sum_\alpha (Y_{\alpha *} - Y_{\alpha e}) h^o_\alpha$$

the adiabatic energy balance between the propellant surface and boundary layer external flow is[9,16]

$$H_e - H_s = \Delta h_g - L_s - c_\pi (T_s - T_i) \tag{11}$$

where $H_e = H_o$ is the constant stagnation enthalpy of the gas. At flow stagnation, the flame temperature is defined as $T_o = H_o/c_p$. Equation (11) is independent of H_s in view of Eq. (10).

New dependent variables are defined such that

$$f_\alpha = \phi^{-1}(Y_\alpha - Y_{\alpha *})/(Y_{\alpha e} - Y_{\alpha *})$$

$$f_H = (H - H_e + \Delta h_g)/(\phi \Delta h_g)$$

Utilizing assumptions (a)-(c), the mass fraction and enthalpy equations (3) and (4) may be written as

$$(\rho f_\alpha)_{,t} + (\rho u^\ell f_\alpha)_{,\ell} = g^{\ell m}(\mu f_{\alpha,m})_{,\ell} + \omega \tag{12}$$

$$(\rho f_H)_{,t} + (\rho u^\ell f_\alpha)_{,\ell} = g^{\ell m}(\mu f_{H,m})_{,\ell} + \omega + (\phi \Delta h_g)^{-1}\left[p_{,t} + (\mu u^m u^\ell_{,m})_{,\ell}\right] \tag{13}$$

The boundary conditions for f_α and f_H (=f, say) may both be written as

$$f_s = (\dot{m}_s)^{-1} \mu n^j f_{,j}\Big|_s \tag{14}$$

at the surface, and

$$f = 1/\phi \tag{15}$$

at the boundary layer edge. It is also assumed that:

d) The term in brackets in Eq. (13) is negligible for the turbulent boundary layer flow of interest. This will be discussed further on in the text.

Hence, Eqs. (12) and (13) imply that $f_\alpha = f_H$ throughout the region bounded by Eqs. (14) and (15), or by a surface where this condition is imposed. This result is important, since it allows a linear relation between both the mean and fluctuating (turbulent) components of Y_α and H in the boundary layer. Specifically, Reynolds averaging[18] yields

$$\bar{Y}_\alpha = Y_{\alpha e} + (Y_{\alpha e} - Y_{\alpha *})(\bar{H} - H_e)/\Delta h_g \qquad (16)$$

$$Y'_\alpha = (Y_{\alpha e} - Y_{\alpha *})H'/\Delta h_g \qquad (17)$$

The analysis of turbulence follows the second-order closure approach rather than the use of an eddy-diffusivity to model turbulence effects. The reasons for using the second-order approach include:

1) Measurements of turbulence in a cold flow simulation of an axisymmetric grain port have been reported by Yamada, et al.[19] Their results show that while the mean longitudinal-velocity profile apparently achieves similarity, the mean-turbulence profile continues to increase in magnitude and move closer to the port surface with distance from the head end. This nonsimilarity between turbulence and mean velocity precludes consideration of customary formulations of eddy diffusivity.[18]

2) If an eddy diffusivity (or mixing length) formulation is assumed, it would have to include the effects of mass injection, viscous sublayer dissipation, and large streamwise pressure gradient on turbulent transport. These effects are fundamentally included in the second-order closure approach.

3) The second-order closure approach has been successfully applied to a variety of flows,[11,20-22] and is therefore not empirically particularized for application to erosive burning.

Since application of the turbulence modeling to boundary-layer-like flows is intended, the basic compressible-flow equations and numerical solution technique of Sullivan[23] will be modified to accommodate propellant combustion. Sullivan considers an energy equation for $h = c_p T = H - u^i u_i/2$, which can be derived by subtracting the equation for kinetic energy from Eq. (4). Therefore, the chemical heat release term in Eq. (4) must be added to the basic enthalpy equation of Sullivan, with the mass fractions related by the present Eqs. (16) and (17). Turbulence analysis proceeds by decomposing all dependent variables into their mean and fluctuating parts (e.g., $h = \bar{h} + h'$). Equations for second-order turbulence variables are derived by cross-correlating the equations for the fluctuating variables. The several indeterminate correlations generated in this process are then modeled in terms of the principal second-order correlations for which differential equations are retained. An evaluation of the turbulence modeling for nonreactive flows using the computer code of Sullivan is given by Rubesin, et al.[22] This reference also lists the models used to close the system, and the values of the turbulence modeling parameters used in the present analysis.

It is now convenient to refer to a Cartesian system with spacial coordinates $\{x,y,z\}$, and velocities $\{u,v,w\}$. Additional assumptions are that:

e) The flow is quasi-steady (e.g., $\bar{h}_{,t} = 0$) , and two-dimensional ($\partial/\partial z = 0 = \bar{w}$) .

f) The flow is of boundary layer type, with outer boundary conditions and static pressure specified by asymptotic matching to an isentropic, one-dimensional flow. It is noted that measurements in cold-flow simulations of planar and axisymmetric grain ports[19,24] indicate that the central flow is two-dimensional. The assumption of a one-dimensional outer flow implies that some error is inherent in applying the present analysis (or those of Ref. (2) and (6)) to grain port flows.

g) Turbulent correlations involving the chemical source term are taken to be zero in the present analysis. This assumption is invoked because complete and consistent models for ω' correlations are unavailable. Such models are under development by Varma, et al.[21] and other investigators. The difficulty in obtaining simple models of the ω' correlations is predominantly due to the inaccuracy of Taylor expansion of the Arrhenious exponential factor. The potential effect of these correlations is probably not negligible, and they may account for "negative erosivity."[25]

Final Equations

Under assumptions (a) - (g), the final system consists of coupled differential equations for $\bar{u}$, $\bar{v}$ (from mean continuity), $\bar{h}$, $\overline{u'u'}$, $\overline{u'v'}$, $\overline{v'v'}$, $\overline{w'w'}$, $\overline{\rho'u'}$, $\overline{\rho'v'}$, $\overline{h'u'}$, $\overline{h'v'}$, and

$\overline{h'h'}$. The second-order correlation equations are quite lengthy and are not listed here. They correspond with the correlation equations of Sullivan but with the terms $\phi\Delta h_g\overline{\chi'\omega'}$ (where χ' represents u' , v' , w' , $2h'$) added to the right-hand sides of the $\overline{h'u'}$, $\overline{h'v'}$, $\overline{h'w'}$ and $\overline{h'h'}$ equations. In accordance with assumption (g), $\overline{\chi'\omega'}$ is taken to be zero. The mean equations for conservation of mass, momentum, enthalpy and the equation of state are

$$(\bar{\rho}\bar{u})_{,x} + (\bar{\rho}\bar{v} + \overline{\rho'v'})_{,y} = 0 \tag{18}$$

$$\bar{\rho}\bar{u}\bar{u}_{,x} + (\bar{\rho}\bar{v} + \overline{\rho'v'})\bar{u}_{,y} + (\overline{\rho u'v'})_{,y} = -\bar{p}_{,x} + (\bar{\mu}\bar{u}_{,y})_{,y} \tag{19}$$

$$\bar{\rho}\bar{u}\bar{h}_{,x} + (\bar{\rho}\bar{v} + \overline{\rho'v'})\bar{h}_{,y} + (\bar{\rho}\,\overline{h'v'})_{,y} = \bar{u}\bar{p}_{,x} + \bar{\mu}\left[(\bar{u}_{,y})^2 + \frac{q^2}{\Lambda^2}\left(a + b\,\frac{\bar{\rho}q\Lambda}{\bar{\mu}}\right)\right] + (\bar{\mu}\bar{h}_{,y})_{,y} + \phi\Delta h_g\bar{\omega} \tag{20}$$

$$\bar{p} = R\bar{\rho}\bar{T}\left[\sum_\alpha \bar{G}_\alpha\left(1 - \overline{T'T'}/\bar{T}^2\right) - \left(\sum_\alpha \overline{G'_\alpha T'}\right)/\bar{T} - \sum_\alpha\sum_\beta \left(\overline{G'_\alpha G'_\beta}\right)/\sum_\alpha \bar{G}_\alpha\right] \tag{21}$$

In Eq. (21), $G_\alpha = Y_\alpha/W_\alpha$, and the assumption that $|p'|$ is relatively small has been used in the derivation.

Considering the effects inherent in Eq. (20), the first two terms on the left side represent the convection of sensible enthalpy in both the streamwise and surface-normal directions. The third term is the turbulent heat flux (to second-order) within the boundary layer. This term is classicially modeled with

the assumption of a turbulent eddy diffusivity, whereas the present analysis carries an independent equation for the development of $\overline{h'v'}$. Following the flow-work $(\overline{up}_{,x})$ term on the right-hand side is a bracketed expression which represents the contribution of viscous dissipation by both the mean and turbulent flow. The term involving $q = (\overline{u'u'} + \overline{v'v'} + \overline{w'w'})^{1/2}$ is the result of modeling the turbulent dissipation. The empirical parameters a and b are equal to $.125$ and 3.25, and Λ is the turbulent length scale. Finally, the last two terms in Eq. (20) are the contributions of the molecular transport of heat, and the volumetric rate of heat production. Using Eqs. (16) and (17), the source term of assumption (c) may be written as

$$\bar{\phi\omega} = B_g \bar{T}^{-\beta_g} \exp(-T_{Ag}/\bar{T})\, \bar{\rho}^{\Phi_F} \left(\frac{H_e - \bar{H}}{\Delta h_g}\right)^{\Phi_F} + \Phi_0$$

where

$$B_g = \phi A_g (Y_{F*}/W_F)^{\Phi_F} (Y_{0*}/W_0)^{\Phi_0}$$

The validity of assumption (d) is now considered, for which it is convenient to refer to the enthalpy equation in its original form (Eq. 4). The magnitudes of the last two terms are assessed for both their mean and turbulent contributions. The contribution of $\bar{p}_{,t}$ is therefore zero under assumption (e), while assumption (f) implies that

$$\left| \left[\bar{\mu} (\overline{uv}_{,x} + \overline{vv}_{,y}) \right]_{,y} \right| << \left| (\mu \overline{u^2}_{,y})_{,y} \right|$$

The turbulent contribution (to the mean equation) of the term $\overline{(\mu u'^{m} u'^{\ell}_{,m})}_{,\ell}$ can be shown to be small relative to $g^{\ell m}\left[\mu\overline{(u'^{1}u'_{i})}_{,m}\right]_{,\ell}$ after substitution of the modeling used in Ref. 23. Correlations of the fluctuating parts of the last two terms in Eq. (4) with any of the dependent variables (e.g., h') are also small relative to the thermal energy correlations for the low Mach numbers obtained in grain ports.

Boundary Conditions

The surface boundary conditions for Eqs. (18)-(20) and the turbulent correlation equations are

$$\bar{v}_s = \bar{\dot{m}}_s/\bar{\rho}_s \ , \ \bar{u}_s = 0 \quad \text{and} \quad \bar{h}_s = c_p \bar{T}_s(\bar{\dot{m}}_s)$$

All correlations are assumed zero at the surface. A linear pyrolysis relation[16]

$$\bar{\dot{m}}_s = A_\pi \bar{T}^{\beta_\pi} \exp(-T_{A\pi}/\bar{T}_s)$$

is used in conjunction with the interface condition, Eq. (9)

$$\bar{\dot{m}}_s = \left[L_s + c_\pi(\bar{T}_s - T_i)\right]^{-1} \frac{k}{c_p} \bar{h}_{,y}\Big|_s$$

to determine $\bar{\dot{m}}_s$ and $\bar{T}_s$.

The asymptotic boundary conditions applied as $y \to \infty$ are:

$$\bar{u} = U_e(x) \quad \text{and} \quad \bar{h} = h_e(x)$$

All correlations are assumed to be zero in the external stream, with the exception that $\overline{u'u'} = \overline{v'v'} = \overline{w'w'} = 10^{-3}(U_e^o)^2$. The parameter $U_e^o = U_e\ (x = 0)$ is specified by the initial conditions. To simulate the effect of propellant-induced longitudinal flow in the channel, a one-dimensional overall mass balance is used, viz.

$$U_e(x) = \frac{\rho_e^o U_e^o}{\rho_e} + \frac{2}{\rho_e s} \int_o^x \dot{\bar{m}}_s \, dx$$

Isentropic relations appropriate for the one-dimensional flow of a perfect gas are used to obtain $h_e(x)$ and $\bar{p} = p_e(x)$ from U_e, upon specification of the stagnation enthalpy, H_o, and pressure, p_o.[26]

Initial Conditions

The initial conditions at $x = 0$ are determined in the following manner. With $U_e = U_e^o = 100$ m/sec, $T = \text{constant} = 2900^oK$, and the viscosity relation of Table 1, a laminar boundary layer with external turbulence is used to start the calculations. Then, the profiles of mean velocity and turbulence correlations are computed at $\xi = 4$ cm (cf. Fig. 1). The Reynolds number based on ξ, U_e^o and T_o is approximately 10^7. For other values of U_e^o, the boundary layer thickness of .179 cm at $x = 0$ is taken to be constant (which would correspond to altering ξ), and the initial profiles of $\bar{u}$ and the velocity correlations are scaled by $U_e^o/100$ m/sec and $(U_e^o)^2/10^4$ m^2/sec^2, respectively. The initial profile for $\bar{h}$ is given by $\bar{h} = H_o - \bar{u}^2/2$. Near the surface, the $\bar{h}$ profile is faired to avoid prescribing an infinite heat transfer to the propellant at $x = 0^+$. Profiles of the enthalpy and density correlations at $x = 0$ are taken to be zero. The initial profiles of pertinent variables are graphically described in Figs. 7 and 8, which will be discussed below. Preliminary calculations have indicated that the shapes of the initial profiles affect the propellant recession rate only over a distance of several initial boundary layer thicknesses.

RESULTS AND DISCUSSION

Physical Parameters

The final form of the turbulent aerothermochemical system contains many physical parameters, most of which may be assigned representative values. Values of the parameters held fixed in the present analysis are listed in Table 1. The flame temperature, propellant density, specific heats and average (product) molecular weight are appropriate to JPN, according to Wimpress.[27] The viscosity relation is used in the analysis of Tien, et al.[28] The pyrolysis constants A_π , β_π and $T_{A\pi}$ are believed typical of those used for propellant stability studies, and yield a surface temperature $T_s = 725^oK$ when $\dot{r} = 1$ cm/sec . The heat of decomposition at reference condition (L_s^o , 0^oK) is considered to be exothermic by at least -100 cal/gm for a monopropellant such as ammonium perchlorate.[29] However, an apparently intrinsic (nonnumerical) instability was noticed in some preliminary computations when L_s^o was less than about -50 cal/gm . The value of -20 was selected to ensure stability over a range of physical conditions.

Table 2 lists the parameters varied in the present study and the corresponding computer run numbers. For each of the thermodynamic or kinetic parameters varied, the normal (nonerosive, steady-state) burning rate was first obtained by solving the energy equation (20) alone, with no ambient turbulence and with the term $\overline{\rho u h}_{,x}$ replaced by $\overline{\rho h}_{,t}$. It was found that the normal burning rate for all conditions in Table 2 could

be represented by $\dot{r}_n/\dot{r}_* = (p/p_*)^n \pm 5\%$, over the range $.5 \leq p/p_* \leq 2$. Table 2 also gives the values of $\dot{r}_*$ (normal burning rate at $p_* = 6.9 \times 10^7$ dyne/cm^2) and n .

External Velocity Effect

Figure 2 shows the effect of constant boundary layer edge velocity, $U_e = U_e^o$, on propellant recession ratio, $\dot{r}/\dot{r}_n$, as a function of distance, x , along the propellant surface. There is a significant (≈30%) reduction in burning rate over the first 10 cm of propellant. A similar decrease was noticed in the composite propellant experiments of Marklund and Lake.[30] Their apparatus produced an approximately constant "crossflow" velocity over a 7 cm-long propellant test strip. This downstream decrease in burning rate for constant edge velocity boundary layers will be shown to be caused by the rapid growth in viscous sublayer thickness. Figure 2 also shows that the normal burning rate is recovered at $U_e = 200$ m/sec for $x > 30$. This location corresponds with the velocity boundary layer detaching from the propellant surface (i.e., exhibiting no surface skin friction). This "blowoff" behavior was discussed by Jeromin,[31] and occurs in turbulent boundary layers with sufficiently large surface-to-edge mass transfer ratios. Edge velocities less than 100 m/sec were investigated, but for these values the boundary layer detached almost immediately. No evidence of "negative erosion"[1] was found in the low U_e investigation.

Channel Width Effect

Figure 3 shows the results of varying the channel width, s, to provide a propellant-induced velocity increase along the channel. The departure from a linear x dependence of U_e (Fig. 3a) is due to the erosive burning effect. The severity of erosive burning for the narrower channel widths ($s = .5, .7$ cm) is noted in Fig. 3b. The value of $s = .7$ is approximately equal to the initial .64 cm width of the rectangular grain port of Peretz, et al.[32] However, an obvious problem arises in the use of small channel widths while also using asymptotic boundary conditions for the dependent variables. The velocity boundary layer thickness for Run 9 ($s = .50$ cm) grows from its initial value of .179 cm to .937 cm at $x = 100$. Most of the growth occurs over the first 10 cm of propellant, with the growth rate diminishing rapidly as the velocity along the channel increases. Despite the large velocity boundary layer thickness, the momentum and displacement thicknesses remain smaller than the channel half-width. It is therefore believed that the results obtained for the finite values of s qualitatively reflect the conditions found in small port diameter motors.

Comparison of Results for Constant Velocity and Accelerated Flows

Figure 4 shows the recession ratio as a function of boundary layer edge velocity, U_e. The propellant properties are identical for each of the velocity response curves shown. The dashed lines are the constant U_e calculations of Fig. 2. These may be considered to represent the recession ratio results of a propellant tested with driver flow apparatus. The solid lines

are the varying U_e calculations of Fig. 3, and simulate, for example, the results of interrupted burning experiments in two-dimensional grain ports. It is apparent that velocity alone is insufficient to scale the recession ratio calculations, even at approximately constant static pressure. The calculations for constant U_e are dependent on downstream position (as in the strip method of Marklund and Lake), while those for varying U_e exhibit a channel width effect. Both effects should be accounted for in predicting full-scale motor performance from erosive burning test data.

In the absence of convective flow, the present theory essentially reduces to the steady-state monopropellant (pure ammonium perchlorate) deflagration theory of Johnson and Nachbar. Nevertheless, the erosive burning results of Fig. 4 are similar in shape to the experimental results obtained by Wimpress (for double-base propellants) and Marklund and Lake (for composite propellants). The present calculations for recession ratio as a function of external velocity generally fall below observed values[1] by a factor of about two for low burning rate propellants. Figure 4 also displays the generally observed phenomenon[1,2,3] of threshold velocity (velocity below which $\dot{r}/\dot{r}_n \leq 1$). Calculated boundary layer profiles (to be discussed) show that threshold velocity is associated with sufficient turbulence entering the flame zone, as hypothesized by Corner.[4]

Pressure Effect

Figure 5 shows the effect of a $\pm 50\%$ variation of stagnation pressure (p_o) on recession ratio, for three values of burning

rate pressure exponent, n. The values of n are obtained by altering the overall reaction order ($\Phi_F + \Phi_0$), while maintaining constant $\dot{r}_*$. For $n = .8$, slight pressure dependence is observed. This is consistent with the experimental observations of Wimpress for homogeneous propellants with similar values of pressure exponent. For $n = .5$ (a value which is more in line with composite propellants) a pronounced effect of pressure on recession ratio is seen in the calculations. The trend for this lower pressure exponent is such that for constant velocity, propellant erosion increases with increasing stagnation pressure. Similar pressure trends have been experimentally observed, particularly for composite propellants.[1,2,30] Results for a pressure exponent of 1.5 show a reversal of the pressure trend, since the recession ratio decreases as p_o increases. The calculations of Fig. 5 additionally indicate that as the pressure exponent decreases, the downward curvature of the recession ratio at higher velocities increases. This nonlinear behavior (i.e., $\dot{r}/\dot{r}_n \sim U_e^m$, $m < 1$) is typical of experimental results.[2,27,30]

Normal Burning Rate Effect

It is well established[26,27,30] that higher burning rate propellants exhibit less tendency toward erosion. This effect is shown by the calculations in Fig. 6. The reference normal burning rate, $\dot{r}_*$, is altered by adjusting the reaction pre-exponential factor B_g. The slope of the velocity response above threshold ($\partial\dot{r}/\dot{r}_n/\partial U_e$) is shown to diminish with increasing $\dot{r}_*$. This is

consistent with the trend observed by Green for composite and homogeneous propellants. It has also been generally observed[1,3] that the threshold velocity increases with normal burning rate - a trend with which the calculations agree.

Boundary Layer Profiles

The previous discussion concerned erosive burning trends which are of engineering importance and which have demonstrated some of the capabilities of the basic theoretical approach. Attention is now given to a discussion of theoretical results which are unavailable from prior erosive burning models. Figure 7 shows the boundary layer profiles of mean temperature and longitudinal velocity component, and the correlations $\overline{h'v'}$ and $\overline{u'v'}$. Note that the quantities $\bar{\rho}\,\overline{h'v'}$ and $-\bar{\rho}\,\overline{u'v'}$ are the turbulent fluxes (to second order) of heat and momentum within the boundary layer. The profiles at various values of x indicate the downstream development of a constant edge velocity (U_e = 400 m/s) boundary layer. As mentioned earlier in the paper, the mean temperature profile at $x = 0$ is selected to represent the initial condition of driver flow combustion products flowing over a cooler propellant surface. The temperature quickly adapts to a quasi-steady state profile by x = 1 cm, a position at which there is approximately 60% erosion (cf. Fig. 2). By $x = 50$, the slope of the temperature profile close to the surface has decreased to provide 20% erosion.

The profiles of $\overline{h'v'}$ (Fig. 7b) show a rapid development from their initial value (assumed zero) to a peak in the neighborhood of $x = 1$. The mechanism of development is

associated with amplification of small values of the velocity correlation, $\overline{u'v'}$, by the large temperature gradient in the flame zone (cf. Fig. 7a,c). The $\overline{h'v'}$ profiles at $x = 10$ and 50 show a decreasing peak value due to a corresponding decrease of $\overline{u'v'}$ in the flame zone (Fig. 7d). This behavior of $\overline{u'v'}$ in the lower boundary layer is in turn caused by a progressive decrease in mean velocity profile gradient (Fig. 7c), which is responsible for the production of $\overline{u'v'}$ in the second-order turbulence equations. It is also noted that the velocity profile develops into a form which is not characterizable by the customary sublayer-logarithmic formulation.[18]

Boundary layer development in a rapidly accelerating flow is significantly different than in the constant external velocity case. Figure 8 shows the profile results of an accelerated flow produced in a channel simulation with $s = .5$ cm. The mean temperature profile develops from its initial state at $x = 0$ (as in Fig. 7a) to a profile which is almost identical to that obtained for normal burning at $x = 1$ cm. The velocity profile gradient increases in the downstream boundary layer (Fig. 8c), and causes a corresponding increase in the turbulent shear stress correlation, $\overline{u'v'}$. The larger amounts of turbulence now entering the flame zone increase the magnitude of the turbulent heat transfer correlation, $\overline{h'v'}$, and move the location of minimum $\overline{h'v'}$ inward. This process apparently causes erosive burning to commence, as is noted from the results of Run 9 in Fig. 3b. The effect of significant $\overline{h'v'}$ is to broaden the temperature profile in the flame zone, as seen in the profiles at $x = 50$ and 75. The phenomenon of flame zone broadening is

associated with small-scale turbulence effects on homogeneous premixed flames.[13]

Comparison of the temperature profile at $x = 75$ with the results of Fig. 3 shows that the observed increase in temperature gradient provides an 85% increase in recession rate. The ratio of the maximum value of turbulent heat transfer to molecular heat transfer in the boundary layer $(-\bar{\rho}\,\overline{h'v'})_{max}/(\overline{kT}_{,y})_{max}$, is approximately 1.7 at $x = 75$. This ratio represents the maximum turbulent to molecular "diffusivity," and is nearly equal to the value of local recession ratio. Figure 8b also shows an appreciable positive value of $\overline{h'v'}$ in the outer portion of the boundary layer at $x = 75$. The temperature at the boundary layer edge at this point has dropped to 2810°, and hence $\bar{\rho}\,\overline{h'v'}$ is transporting heat away from the flame zone, toward both the propellant and the central channel flow. However, the length scale of the positive outward heat flux is much larger (by a factor of 10^2) than the length scale of the negative heat flux to the propellant. This may explain the insensitivity of recession ratio to driver flow temperature, as observed by Marklund-Lake and Wimpress.

SUMMARY

Solid propellant erosive burning has been investigated using a reacting turbulent boundary layer approach. An advantage of this approach over current methods is that it does not *a priori* assume a specific causal mechanism for erosive burning. Rather, most previously speculated causes are fundamentally described by the governing differential equations. The important details of turbulence development are obtained with the second-order closure technique, and a single-step global reaction is assumed for the combustion of a homogeneous propellant. In the absence of convective flow, the present combustion model essentially reduces to that of Johnson and Nachbar, which was developed for a monopropellant. As no experimental results have been reported for monopropellant erosive burning, the present analysis is restricted to the consideration of erosive burning trends which are observed for most propellant types.

The theoretical method is found to be in agreement with the generally observed trends of threshold velocity, nonlinear recession-ratio velocity dependence, pressure dependence, and normal burning rate sensitivity. The theory displays the transient erosive burning effect noted in the experiments of Marklund and Lake, and also exhibits a dependence on channel width in simulations of motor port flow.

The ability of the theory to provide boundary layer profiles of the mean and turbulent fields has been utilized to investigate the cause of erosive burning for the combustion mechanism assumed. Consistent with classical concepts, erosive burning appears

coincidentally with turbulence entering the flame zone. The mechanism of increased surface heat transfer is associated with the broadening of the flame zone due to the diffusive effects of turbulence.

REFERENCES

1. Williams, F.A., Barrere, M., and Huang, N.C.: "Fundamental Aspects of Solid Rockets," AGARDograph No. 116, Chapters 4, 6 and 7, Oct. 1969, pp. 339-456.

2. King, M.K.: "A Model of Erosive Burning of Composite Propellants," *AIAA/SAE 13th Propulsion Conference*, Paper No. 77-930, July 1977.

3. Kuo, K.K. and Razdan, M.K.: "Review of Erosive Burning of Solid Propellants," *Proceedings of the 12th JANNAF Combustion Meeting*, Aug. 1975, pp. 323-338.

4. Corner, J.: "The Effect of Turbulence on Heterogeneous Reaction Rates," *Trans, Faraday Soc.*, Vol. 43, 1947, pp. 635-642.

5. Vandenkerckhove, J.A.: "Erosive Burning of a Colloidal Solid Propellant," *Jet Propulsion*, Vol. 28, Sept. 1958, pp. 599-603.

6. Lengellé, G.: "Model Describing the Erosive Combustion and Velocity Response of Composite Propellants," *AIAA Journal*, Vol. 13, Mar. 1975, pp. 315-322.

7. Lenoir, J.M., and Robillard, G.: "A Mathematical Method to Predict the Effects of Erosive Burning in Solid Propellant Rockets," *Proceedings of the 6th Symposium (International) on Combustion*, Reinhold Pub., 1957, pp. 663-667.

8. Schlicting, H.: *Boundary Layer Theory*, 6th ed., McGraw Hill, Chapter 23, 1968.

9. Tsuji, H.: "An Aerothermochemical Analysis of Erosive Burning of Solid Propellants," *Proceedings of the 9th International Symposium on Combustion*, 1963, pp. 384-393.

REFERENCES (cont.)

10. Schuyler, F.L. and Torda, T.P.: "An Aerothermochemical Analysis of Solid Propellant Combustion," *AIAA Journal*, Vol. 4, Dec. 1966, pp. 2171-2177.

11. Varma, A.K., Beddini, R.A., Sullivan, R.D., and Donaldson, C. duP.: "Application of an Invariant Second-Order Closure Model to the Calculation of Compressible Boundary Layers," *7th Fluid and Plasma Dynamics Conf.*, AIAA Paper No. 74-592, June 1974.

12. Razdan, M.K. and Kuo, K.K.: "Erosive Burning Stuides of Composite Propellants by the Reacting Turbulent Boundary-Layer Approach," Interim Report, Penn, State Univ., Nov. 1976.

13. Williams, F.A.: *Combustion Theory*, Addison-Wesley, Chapters 1, 5, 7, 1965.

14. Aris R.: *Vectors, Tensors and the Basic Equations of Fluid Mechanics*, Prentice-Hall, Inc., 1962.

15. Dryer, F. and Glassman, I.: "High Temperature Oxidation of CO and CH_4," *Proceedings of the 14th Symposium (International) on Combustion*, 1972, pp. 987-1003.

16. Johnson, W.E. and Nachbar, W.: "Deflagration Limits in the Steady Linear Burning of a Monopropellant with Application to Ammonium Perchlorate," *Proceedings of the 8th International Symposium on Combustion*, Williams and Wilkins Co., 1962, pp. 678-689.

17. Glasstone, S.: *Textbook of Physical Chemistry*, 2nd ed., Van Nostrand, Inc. 1946, pp. 453-460.

REFERENCES (cont.)

18. Hinze, J.O.: *Turbulence*, 2nd ed., McGraw-Hill, Chapters 5 and 7, 1975.

19. Yamada, K., Goto., M., and Ishikawa, N.: "Simulative Study on the Erosive Burning of Solid Rocket Motors," *AIAA Journal*, Vol. 14, Sept. 1976, pp. 1170-1177.

20. Lewellen, W.S., Teske, M.E., and Donaldson, C. duP.: "Variable Density Flows Computed by a Second-Order Closure Description of Turbulence," *AIAA Journal*, Vol. 14, Mar. 1976, pp. 382-387.

21. Varma, A.K., Fishburne, E.S., and Donaldson, C. duP.: "Aspects of Turbulent Combustion," *15th Aerospace Sciences Meeting*, AIAA Paper No. 77-100, Jan. 1977.

22. Rubesin, M.W., Crisalli, A.J., Lanfranco, M.J., Horstman, C.C., and Acharya, M.: "A Critical Evaluation of Second-Order Closure Models for Incompressible and Compressible Boundary Layers with Axial Pressure Gradient," *15th Aerospace Sciences Meeting*, AIAA Paper No. 77-128, Jan. 1977.

23. Sullivan, R.D.: "GYC - A Program to Compute the Turbulent Boundary Layer on a Rotating Cone," Aeronautical Research Associates of Princeton, Inc., Working Paper No. 76-2, Aug. 1976.

24. Dunlap, R., Willoughby, P.G., and Hermsen, R.W.: "Flowfield in the Combustion Chamber of a Solid Propellant Rocket Motor," *AIAA Journal*, Vol. 12, Oct. 1974, pp. 1440-1442.

REFERENCES (cont.)

25. Vilyunov, V.N. and Dvoryashin, A.A.: "An Experimental Investigation of the Erosive Burning Effect," *Comb., Expl. and Shockwaves,* 1973, pp. 38-42.

26. Green, L.: "Erosive Burning of Some Composite Solid Propellants," *Jet Propulsion,* Vol. 24, Jan.-Feb. 1954, pp. 9-15.

27. Wimpress, R.N.: *Internal Ballistics of Solid Fuel Rockets,* McGraw-Hill, Chapters 2 and 6, 1950.

28. T'ien, J.S., Sirignano, W.A., and Summerfield, M., "Theory of L-Star Combustion Instability with Temperature Oscillations," *AIAA Journal,* Vol. 8, 1970, pp. 2200-2207.

29. Guirao, C. and Williams, F.A.: "A Model for Ammonium Perchlorate Deflagration Between 20 and 100 Atm," *AIAA Journal,* Vol. 9, July 1971, pp. 1345-1356.

30. Marklund, T. and Lake, A.: "Experimental Investigation of Propellant Erosion," *ARS Journal,* Vol. 30, Feb. 1960, pp. 173-178.

31. Jeromin, L.O.F.: "An Experimental Investigation of the Compressible Turbulent Boundary Layer with Air Injection," Aeronautical Research Council, R & M No. 3526, 1968.

32. Peretz, A., Kuo, K.K., Caveny, L.H., and Summerfield, M.: "Starting Transient of Solid-Propellant Rocket Motors with High Internal Gas Velocities," *AIAA Journal,* Vol. 11, Dec. 1973, pp. 1719-1727.

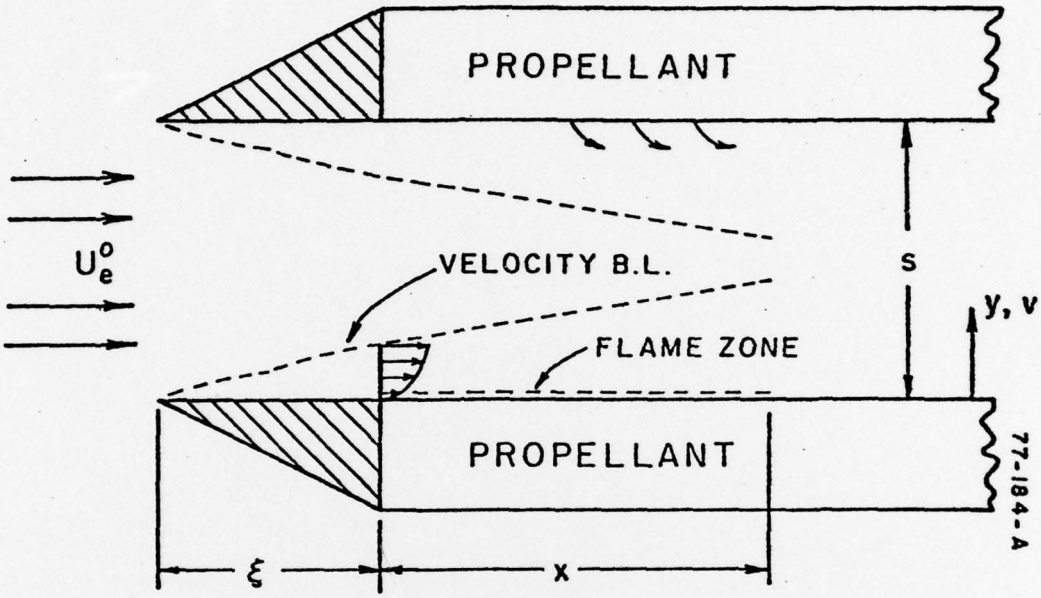

Figure 1. Schematic of the erosive burning flow geometry.

Table I. FIXED PARAMETERS

$T_o = 2900\ °K$

$c_p = .414\ cal/gm-°K$

$W_\alpha = W = 27.1\ gm/gm-mole$

$T_{Ag} = 2.0 \times 10^4\ °K$

$L_s^o = -2\ 0 cal/gm$

$\beta_g = 0$

$\mu = .87 \times 10^{-6} W^{.5} T^{.65} poise$

$T_i = 300\ °K$

$\rho_\pi = 1.62\ gm/cm^3$

$c_\pi = .35\ cal/gm-°K$

$\beta_\pi = 0$

$A_\pi = 1.588 \times 10^6\ gm/cm^2-sec$

$T_{A\pi} = 1.0 \times 10^4\ °K$

Table 2. COMPUTATIONAL CONDITIONS

Run	P_o $\times 10^{-7}$ dyne/cm^2	B_g *	$\dot{r}$ * cm/sec	$\Phi_F + \Phi_O$	n	U_e^o m/sec	s cm
1	6.897	9.41×10^{10}	.9383	1.6	.808	400	∞
2	↓	↓	↓	↓	↓	100	2.0
3	↓	↓	↓	↓	↓	↓	1.0
4	↓	↓	↓	↓	↓	↓	.7
5	↓	↓	↓	↓	↓	↓	.5
6	↓	4.71×10^{10}	.6684	↓	.807	↓	2.0
7	↓	↓	↓	↓	↓	↓	1.0
8	↓	↓	↓	↓	↓	↓	.7
9	↓	↓	↓	↓	↓	↓	.5
10	↓	↓	↓	↓	↓	↓	∞
11	↓	↓	↓	↓	↓	200	↓
12	↓	↓	↓	↓	↓	300	↓
13	↓	↓	↓	↓	↓	400	↓
14	↓	↓	↓	↓	↓	500	↓
15	↓	↓	↓	↓	↓	600	↓
16	↓	↓	↓	↓	↓	700	↓
17	↓	↓	↓	↓	↓	800	↓
18	10.346	↓	↓	↓	↓	100	.5
19	3.449	↓	↓	↓	↓	100	.5
20	6.987	1.88×10^{11}	1.3387	↓	.790	400	∞
21	↓	↓	↓	↓	↓	100	.7
22	↓	↓	↓	↓	↓	↓	.5
26	6.897	1.25×10^{9}	.6690	1.0	.497	↓	↓
27	10.346	↓	↓	↓	↓	↓	↓
28	3.449	↓	↓	↓	↓	↓	↓
29	6.897	1.13×10^{14}	.6643	3.0	1.50	↓	↓
30	10.346	↓	↓	↓	↓	↓	↓
31	3.449	↓	↓	↓	↓	↓	↓

* Units: $\left[gm^{1-m} cm^{m-1} sec^{-1} {}^{\circ}K^{-\beta_g}\right]$, $m = \Phi_F + \Phi_O$

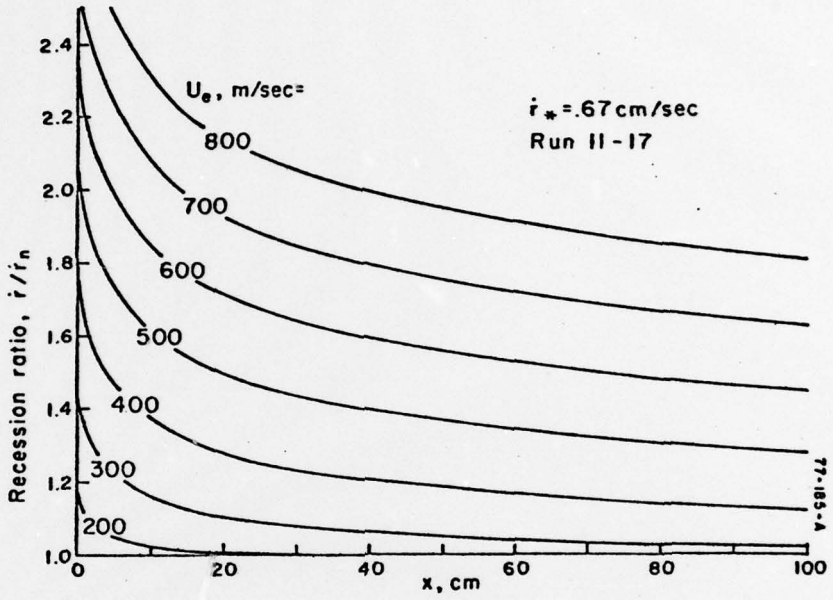

Figure 2. The effect of constant boundary layer edge velocity, U_e, on recession ratio, $\dot{r}/\dot{r}_n$, as a function of distance along the propellant, x.

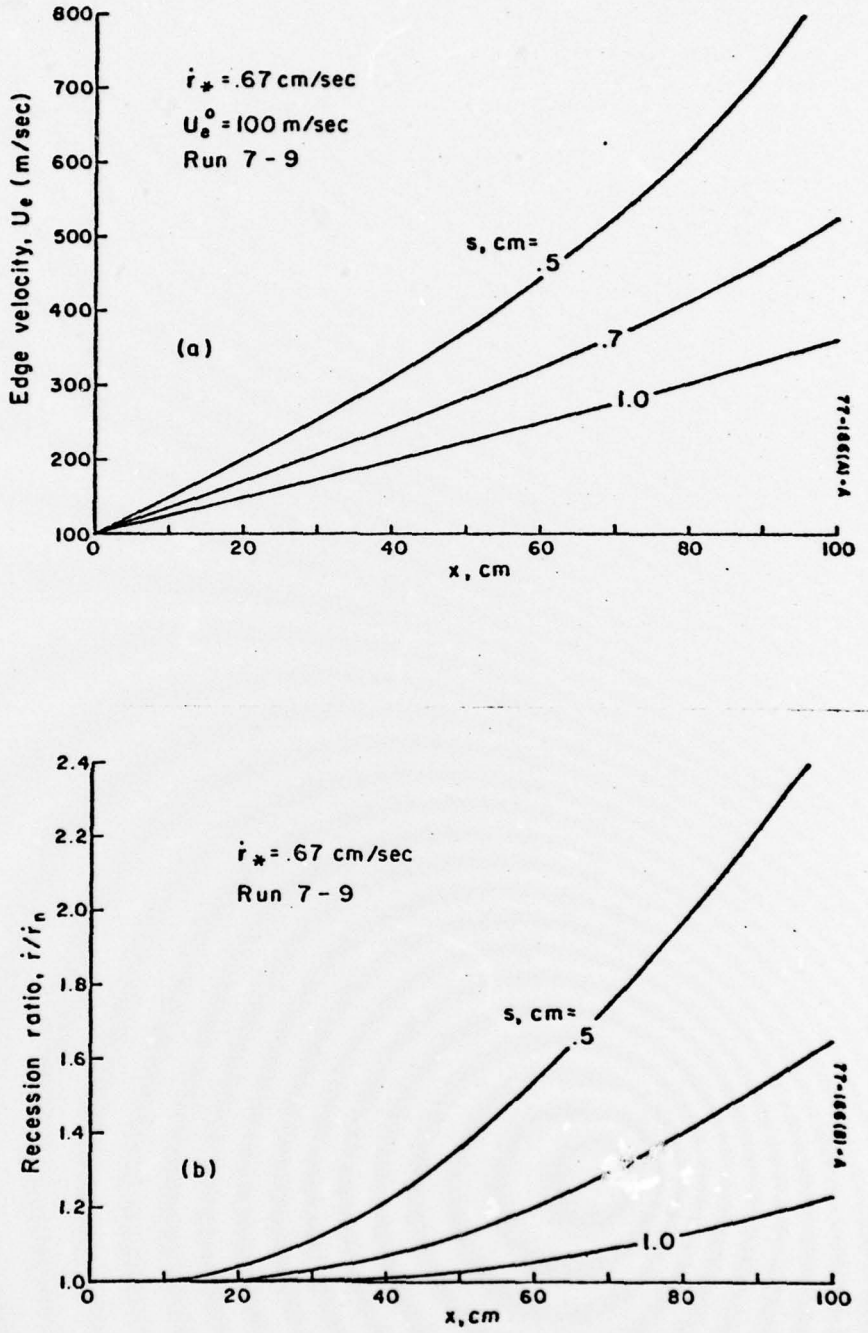

Figure 3. The effect of channel width, s , on a) boundary layer edge velocity, b) recession ratio; as a function of distance along the propellant, x .

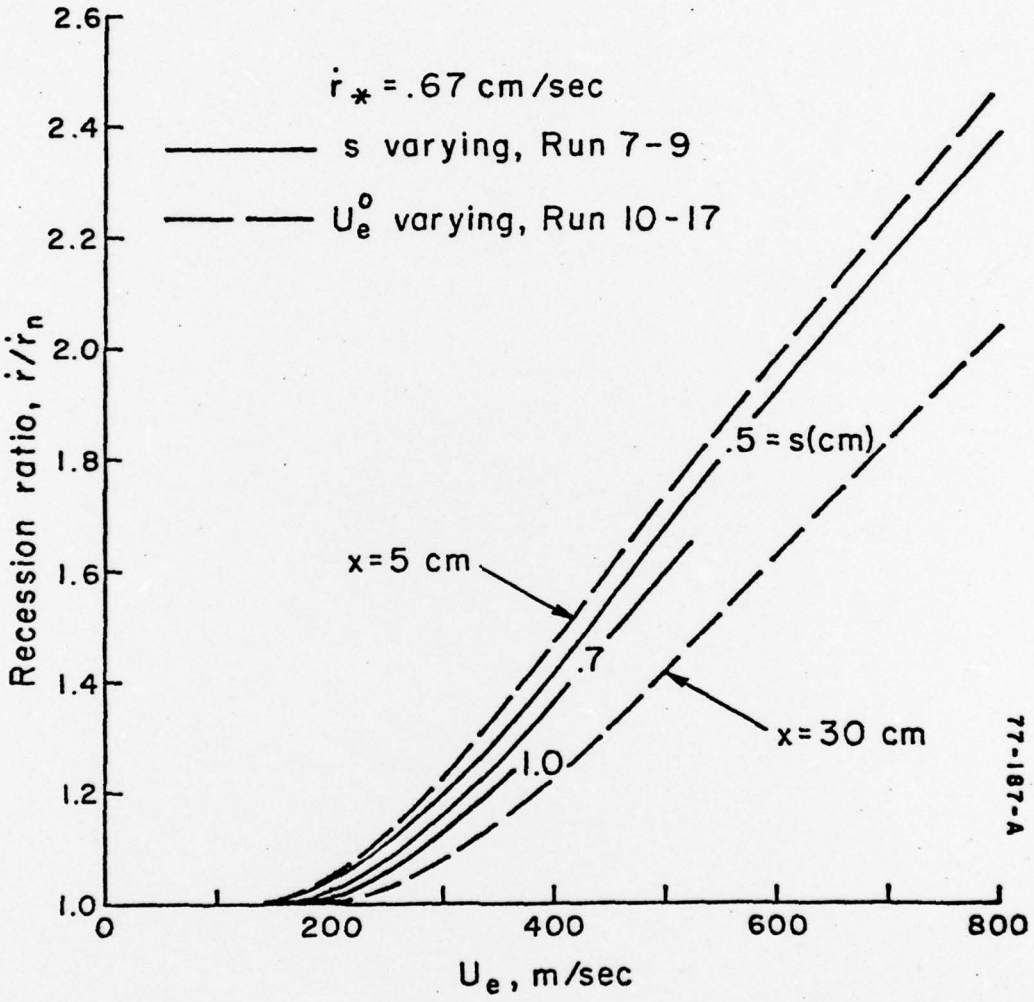

Figure 4. Length scale effects on recession ratio, as a function of boundary layer edge velocity.

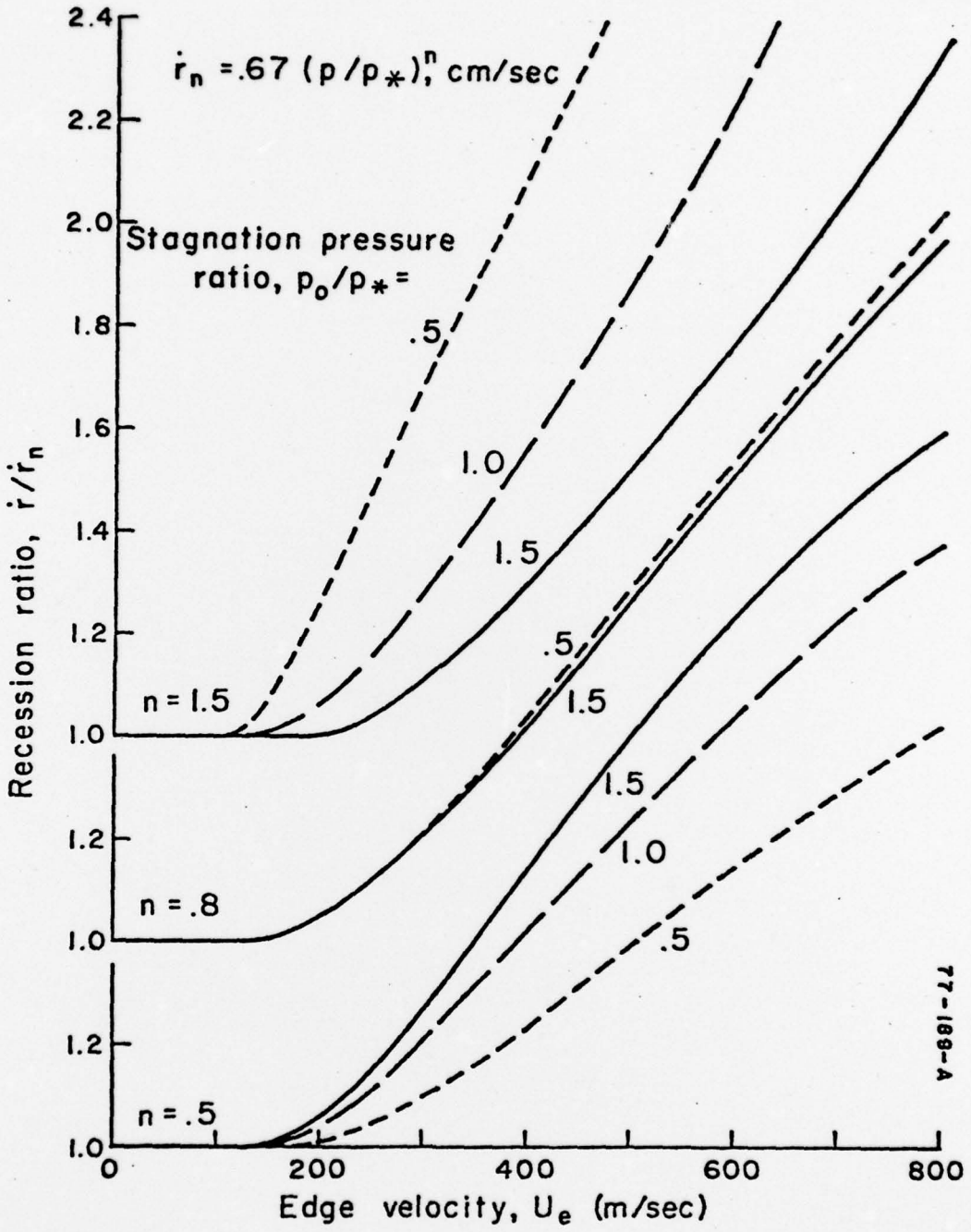

Figure 5. The effects of stagnation pressure (p_o) and normal burning rate pressure exponents (n) on recession ratio.

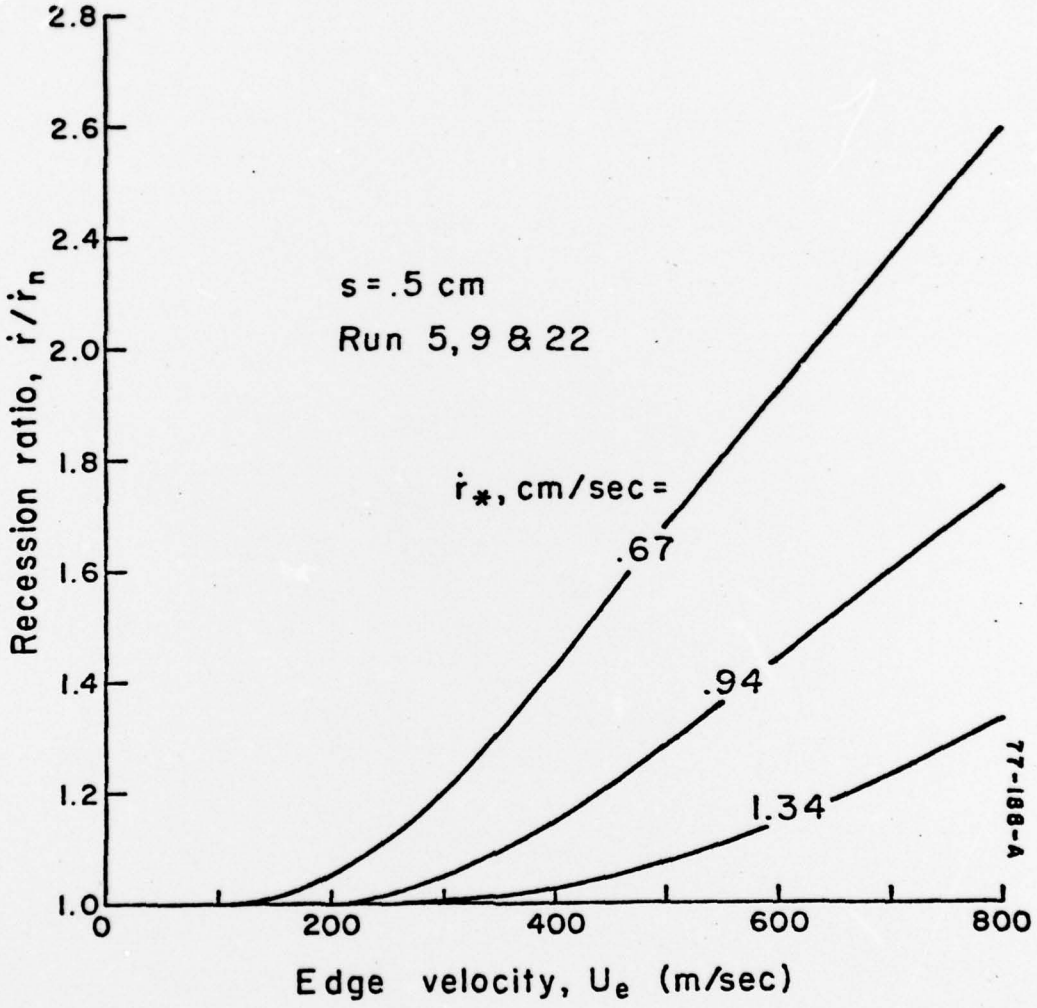

Figure 6. The effect of normal burning rate on recession ratio.

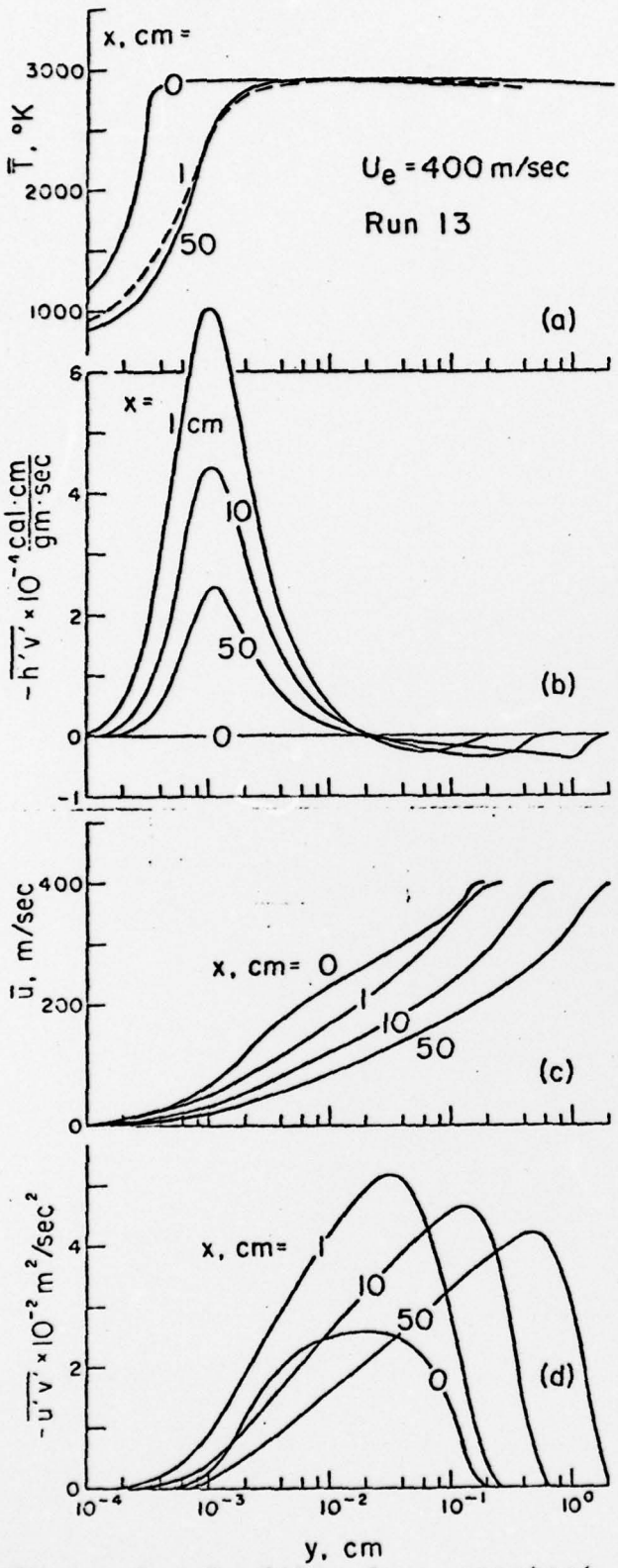

Figure 7. Profiles in a constant edge velocity (U_e = 400 m/sec) boundary layer; a) mean temperature, b) heat transfer correlation, c) mean velocity, d) shear stress correlation.

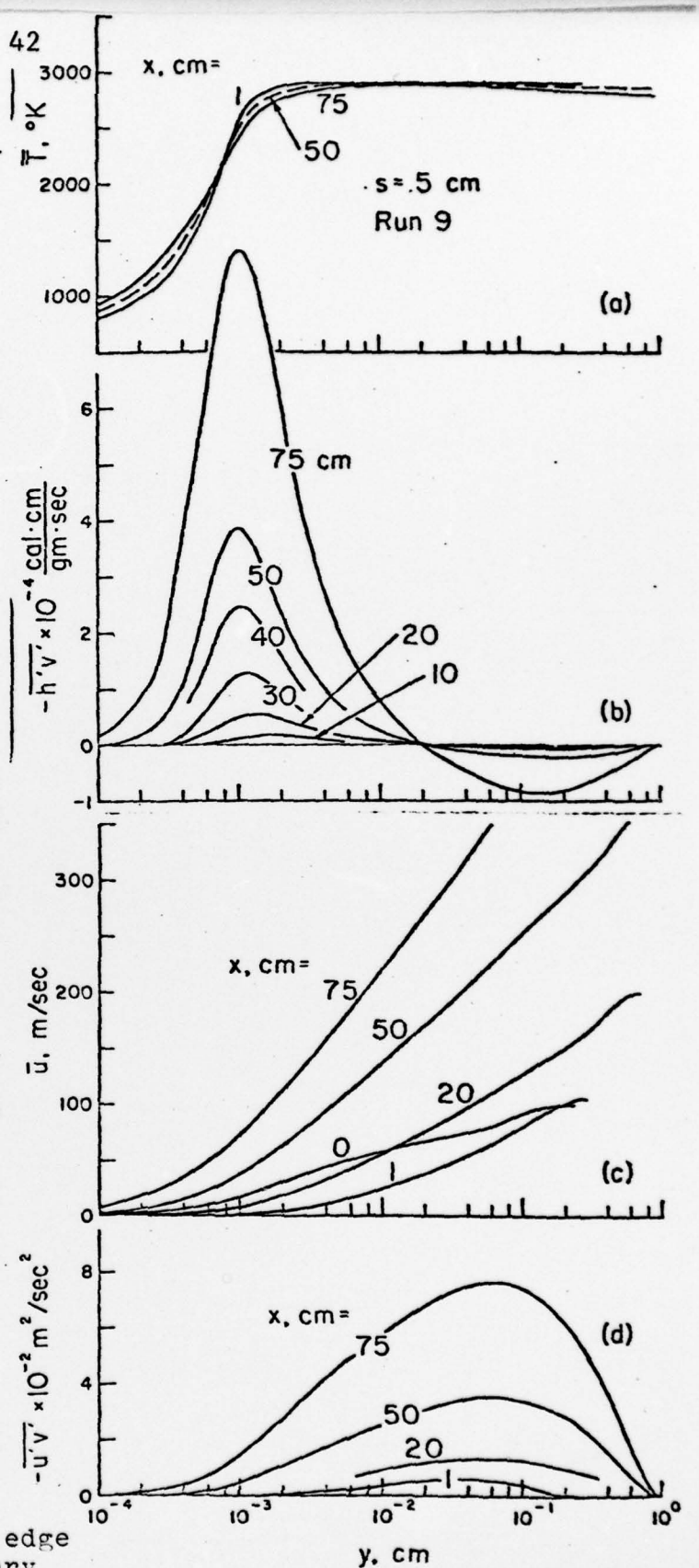

Figure 8. Boundary layer profiles in a channel flow simulation; a) mean temperature, b) heat transfer correlation, c) mean velocity, d) shear stress correlation.